Functional Expression of *Drosophila para* Sodium Channels
Modulation by the Membrane Protein TipE and Toxin Pharmacology

Jeffrey W. Warmke,* Robert A.G. Reenan,‖ Peiyi Wang,* Su Qian,* Joseph P. Arena,§ Jixin Wang,‡ Denise Wunderler,‡ Ken Liu,§ Gregory J. Kaczorowski,‡ Lex H.T. Van der Ploeg,* Barry Ganetzky,‖ and Charles J. Cohen‡

From the *Department of Genetics and Molecular Biology, ‡Department of Membrane Biochemistry and Biophysics, and §Department of Cellular Biochemistry and Physiology, Merck Research Laboratories, Rahway, New Jersey 07065; and ‖Laboratory of Genetics, University of Wisconsin, Madison, Wisconsin 53706

ABSTRACT The *Drosophila para* sodium channel α subunit was expressed in *Xenopus* oocytes alone and in combination with *tipE*, a putative *Drosophila* sodium channel accessory subunit. Coexpression of *tipE* with *para* results in elevated levels of sodium currents and accelerated current decay. Para/TipE sodium channels have biophysical and pharmacological properties similar to those of native channels. However, the pharmacology of these channels differs from that of vertebrate sodium channels: (*a*) toxin II from *Anemonia sulcata*, which slows inactivation, binds to Para and some mammalian sodium channels with similar affinity ($K_d \cong 10$ nM), but this toxin causes a 100-fold greater decrease in the rate of inactivation of Para/TipE than of mammalian channels; (*b*) Para sodium channels are >10-fold more sensitive to block by tetrodotoxin; and (*c*) modification by the pyrethroid insecticide permethrin is >100-fold more potent for Para than for rat brain type IIA sodium channels. Our results suggest that the selective toxicity of pyrethroid insecticides is due at least in part to the greater affinity of pyrethroids for insect sodium channels than for mammalian sodium channels.

KEY WORDS: Na^+ channels • pyrethroid • insecticide • toxin • *Xenopus* oocyte

INTRODUCTION

Voltage-activated sodium channels are transmembrane proteins that provide the current pathway for rapid depolarization of muscles, nerves, and other electrically excitable cells (Hodgkin and Huxley, 1952; Catterall, 1992). Most of our current understanding about the structure and function of sodium channels has come from studying heterologously expressed mammalian sodium channels (Catterall, 1992). Although mammalian sodium channels contain as many as three subunits (α, β_1, and β_2), the ionic selectivity, time and voltage dependence of activation, modulation by protein kinases A and C, and most pharmacological properties are reconstituted by expression of the single core α subunit (Catterall, 1992). Coexpression of the α subunit with the β_1 subunit sometimes enhances expression and alters the time and voltage dependence of inactivation (Isom et al., 1992; Patton et al., 1994). While sodium channels have also been cloned from a variety of invertebrate organisms, little is known about the structure–function relationships of these sodium channel subunits because we and our collaborators (Feng et al., 1995*a*) have only recently identified conditions for heterologous expression of a representative invertebrate sodium channel from *Drosophila*.

Drosophila provides a useful system to study sodium channels because it allows a combination of biophysical, molecular genetic, and transgenic techniques to facilitate both in vivo and heterologous expression studies. The gene encoding a sodium channel α subunit in *Drosophila, paralytic (para)*, has been cloned, and the entire cDNA sequence determined (Loughney et al., 1989; Ramaswami and Tanouye, 1989; Thackeray and Ganetzky, 1994). The predicted polypeptide is ~50% identical to vertebrate neuronal sodium channel α subunits and has four internally homologous domains like those conserved in all other voltage-gated sodium channels (Guy and Conti, 1990; Catterall, 1992). The *para* locus encodes the predominant class of voltage-activated sodium channels expressed in *Drosophila* neurons (Hong and Ganetzky, 1994), and the primary transcript from the *para* gene undergoes a developmentally regulated complex pattern of alternative splicing that potentially generates over 100 different sodium channel isoforms (Thackeray and Ganetzky, 1994; O'Dowd et al., 1995). Relatively little is known about the functional significance of these alternative exons, but the available evidence indicates that the splice variants could provide an important basis for structure-activity studies (O'Dowd et al., 1995*b*). Furthermore, sodium channels

R.A.G. Reenan's current address is Department of Pharmacology, University of Connecticut Health Center, Farmington, CT 06030.

Address correspondence to Dr. Charles Cohen, Merck Research Laboratories, P.O. Box 2000, Rm. 80N-31C, Rahway, NJ 07065. FAX: 908-594-3925; E-mail: cohenc@merck.com

are an important target for insecticides (Vijverberg and van den Bercken, 1990; Bloomquist, 1993; Narahashi, 1996) and expression of insect sodium channels will facilitate a detailed comparative study with vertebrate sodium channels.

Pyrethroids are a widely used class of neurotoxic insecticides that have been shown to interact with many membrane proteins, but their effects on sodium channels are particularly well documented (Vijverberg and van den Bercken, 1990; Bloomquist, 1993; Narahashi, 1996). Some *para* mutants are resistant to pyrethroids, strongly suggesting that the primary site of action is on this sodium channel (Hall and Kasbekar, 1989). Likewise, target-site pyrethroid resistance in house fly, German cockroach, and tobacco budworm all map to the homologous *para* gene in these species (Taylor et al., 1993; Williamson et al., 1993; Dong and Scott, 1994; Knipple et al., 1994; Miyazaki et al., 1996). Although pyrethroids exhibit high levels of toxicity against most arthropods, they have low mammalian toxicity. This specificity of action is critical for their commercial use, but the basis for it is incompletely understood. Grasshopper thoracic ganglion sodium channels are far more sensitive to modulation by pyrethroids than mammalian channels (Ertel et al., 1994). However, some studies suggest that factors unrelated to sodium channel structure, such as the temperature dependence of drug effect, can be important determinants of specificity of action. The greater efficiency of detoxification in mammals also contributes to pyrethroid safety (Narahashi, 1992; Song and Narahashi, 1996). Furthermore, pyrethroids are highly lipophilic and their specificity could derive from a more favorable partition coefficient into insect membranes rather than a difference in the binding site on the channel protein.

To better understand the biophysical and pharmacological properties of insect sodium channels, we identified conditions suitable for heterologous expression of *para* sodium channels in *Xenopus* oocytes. In contrast with previous studies of most mammalian sodium channel α subunits, we found poor expression of *para* alone. Likewise, sodium channels from other invertebrates and lower vertebrates have been cloned but not expressed. We investigated two likely explanations for this poor expression: that only some splice variants will form functional sodium channels and that accessory subunits are necessary for robust functional expression. We found that coexpression of *para* with another *Drosophila* protein encoded by the *tipE* locus results in robust sodium currents (denoted Para/TipE sodium channels; see also Feng et al., 1995*a*). The properties of expressed *Drosophila* sodium channels were compared with those of the rat brain IIA (RBIIA) sodium channel coexpressed with the rat brain β_1 subunit (denoted RBIIA/β1 sodium channels). Para/TipE sodium channels have gating kinetics and pharmacology distinct from rat brain sodium channels. Our studies show that the biophysical and biochemical properties of invertebrate and vertebrate neuronal sodium channels are distinct and provide a system for the analysis of the structure–function relationships that underlie this diversity.

METHODS

Composite para cDNA Construction

General recombinant DNA methods such as DNA ligations, plasmid DNA minipreparation, restriction endonuclease digestion, and agarose gel electrophoresis were all performed using standard methodology (Sambrook et al., 1989).

Because the existing *para* cDNA clones were not suitable for constructing a composite cDNA using conventional cloning techniques, a series of PCR generated cDNA clones were synthesized and assembled on the backbone of the *para* cDNA clone ZS10.3 (Loughney et al., 1989). Oligonucleotide primers used were P1 [5′-GATTCTAGACGTTGGCCGCATAGACAATGACAG-3′], oligonucleotide P2 [5′-GAAGAGCTCGACGAAGGGATCG-3′], oligonucleotide P3 [5′-TCTTCGATCCCTTCGTCGAGCTCT-3′], oligonucleotide P4 [5′-AAAGGATCCAAATATGATGAA-3′], oligonucleotide P5 [5′-TTTGGATCCTTTTTCACACTCAATC-3′], oligonucleotide P6 [5′-GATTCTAGAGCTAATACTCGCGTGCATCTTGG-3′], and P7 [5′-TTGCTGCCAGATCTCATAGTACATG-3′]. PCR (30 cycles) conditions were 1 min at 95°C, 1 min at 55°C, and 2 min at 72°C with reactions containing either primers P1 and P2, P3 and P4, P5 and P6, or P5 and P7 with random-primed adult *Drosophila* cDNA (prepared according to Thackeray and Ganetzky, 1994) as template (see Fig. 1). PCR products of the appropriate size were recovered from agarose gels by electrophoresis onto dialysis membrane (Sambrook et al., 1989), ethanol precipitated, digested with the appropriate restriction enzymes, and ligated into pBluescript SK+ (Stratagene Inc., La Jolla, CA), and the DNA sequence of a number of clones were analyzed (Sequenase 2.0 kit; United States Biochemicals, Cleveland, OH) to identify cDNA clones lacking PCR artifacts. The XbaI/BamHI fragment of the primer 1-2 PCR product was ligated to the BamHI/StuI fragment of ZS10.3 to assemble the 5′ half of the composite cDNA while removing upstream out of frame initiation codons. The StuI/BamHI fragment of the primer 3-4 PCR product was ligated to the BamHI/HindIII fragment of the primer 5-7 PCR product, and this was ligated to the HindIII/XbaI fragment of the primer 5-6 PCR product to assemble the 3′ half of the composite cDNA. Each half of the composite cDNA was then ligated into the pGH19 vector (Liu et al., 1996), which contains the 5′ and 3′ untranslated *Xenopus* beta-globin sequences to stabilize heterologous cRNAs expressed in *Xenopus* oocytes; this construct is designated *para* 13-5. The *para* 13-5 cDNA contains exons j, i, b, d, e, and lacks exons a and f (Fig. 1). A *para* cDNA containing exon a but otherwise identical to 13-5 was constructed by identifying an exon a containing primer 1-2 PCR product and substituting this fragment into the full length *para* 13-5 cDNA as outlined above.

In Vitro Translation of Para

Para protein was synthesized in vitro from the composite *para* cDNA clone using the TNT-coupled reticulocyte system using the manufacturer's protocol (Promega Corp., Madison, WI). Standard SDS/PAGE was carried out according to Laemmli (1970). Kaleidoscope prestained molecular weight standards (Bio-Rad Laboratories, Hercules, CA) were used to determine the appar-

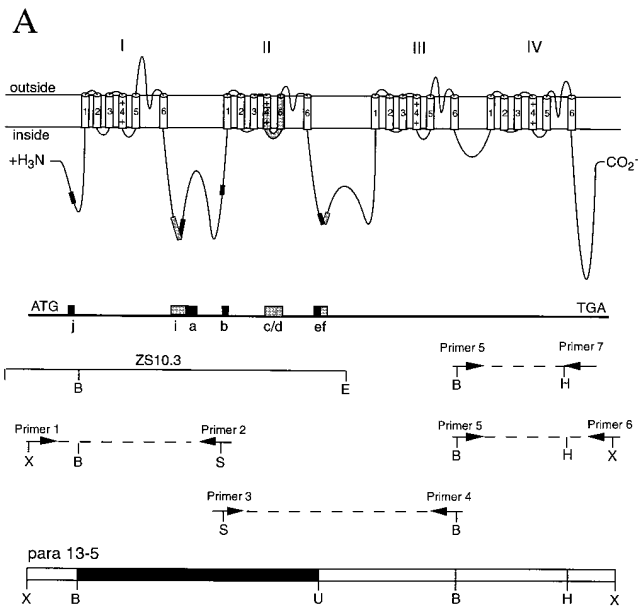

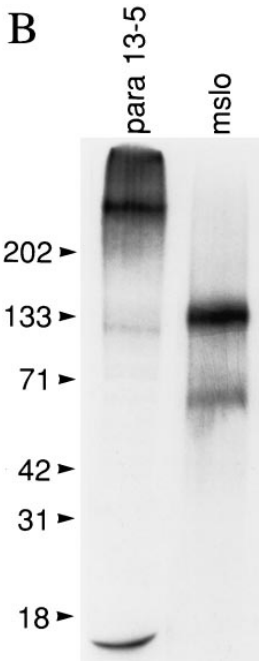

FIGURE 1. *Drosophila para* sodium channel cDNAs. (*A*) Construction of a full length *para* sodium channel cDNA. A schematic representation of the predicted membrane topology of the *para* voltage-activated sodium channel α subunit approximately proportional to its true length with the cylinders representing probable transmembrane α helices. The approximate location of alternative exons are indicated. The location of the *para* ZS10.3 cDNA and the PCR fragments used to construct the full length *para* cDNA clone 13-5 are indicated. The *para* cDNA clone 13-5 is a composite of the ZS10.3 clone (*filled box*) and the PCR-generated cDNA clones (*open boxes*) and was constructed as described in METHODS. The *para* 13-5 cDNA contains exons j, i, b, d, e, and lacks exons a and f. The *para* 13-5 cDNA contains six amino acid substitutions as compared with the previously published sequence apparently due to polymorphisms within and between the Canton-S and Oregon-R strains of *Drosophila melanogaster* (G1158R, R1296Q, D1300N, L1363F, S1587N, and N1822S). Abbreviations for endonuclease restriction enzymes are B, BamHI; E, EcoRI; H, HindIII; S, SacI; U, StuI; and X, XbaI. The alternative exon j encodes amino acids 50–61, which are omitted in some *para* isoforms. Amino acid location is according to the complete *para* amino acid sequence including all known alternative exons (GenBank accession number M32078). (*B*) *In vitro* translation of the *para* voltage-activated sodium channel α subunit. Plasmid DNAs encoding either the *para* voltage-activated sodium channel α subunit or the mouse high conductance calcium-activated potassium channel α subunit were incubated in a rabbit reticulocyte *in vitro* transcription/translation reaction in the presence of [^{35}S]methionine, and the products were run directly on a 4–20% SDS/PAGE and autoradiographed as described in METHODS. The *para* voltage-activated sodium channel α subunit has a predicted M_r of 241 kD and the mouse high conductance calcium-activated potassium channel α subunit has a predicted M_r of 135 kD. The position of M_r markers are indicted on the left.

ent molecular mass of the synthesized proteins. To visualize the [^{35}S]methionine-labeled translation products, the gels were incubated with Enlightning reagent (NEN Research Products, Boston, MA) according to the manufacturer's protocol, followed by autoradiography at room temperature. The mSlo19 cDNA clone (Pallanck and Ganetzky, 1994) encoding a mouse high conductance calcium-activated potassium channel alpha subunit was used as a positive control.

Expression of Sodium Channel cRNAs in Xenopus Oocytes

Capped cRNA transcripts were synthesized using the mMESSAGE mMACHINE in vitro RNA transcription kit (Ambion Inc., Austin, TX). Plasmid vectors encoding the rat brain IIA α subunit (Zem-RVSP6-2580) and rat brain β_1 subunit (p β_1.c1Aa) were obtained from William Catterall (University of Washington, Seattle, WA). cRNA encoding TipE was provided by Linda Hall (State University of New York, Buffalo, Buffalo, NY).

Xenopus laevis oocytes were prepared and injected using standard methods (Arena et al., 1991; Arena et al., 1992; Goldin, 1992). For most experiments, oocytes were injected with 10 ng of each cRNA species being tested (1:1 ratio by weight) in 50 nl RNase-free water. Control oocytes were injected with 50 nl water. For coexpression studies, oocytes were incubated for 2-5 d in ND-96 before recording. When *para* alone was expressed, 50 ng of cRNA was injected and oocytes were incubated for at least 7 d. Incubations and collagenase digestion were carried out at 18–22°C.

The isoleucine isoform of toxin II from *Anemonia sulcata* (ATX-II)[1] and tetrodotoxin were obtained from Calbiochem Corp. (La Jolla, CA). Racemic permethrin and deltamethrin were obtained from Crescent Chemical Co. Inc., (Hauppauge, NY) (U.S. distributor for Riedel-de Haen); they were dissolved in ethanol to make a 10-mM stock solution.

Most voltage-clamp studies were conducted with the cut-open oocyte technique (Taglialatela et al., 1992) using a Dagan CA1 amplifier (Dagan Instruments, Minneapolis, MN). Oocytes were permeabilized with 0.1% saponin and dialyzed with an intracellular solution consisting of (mM): K glutamate 100, HEPES 10, EGTA 1, adjusted to pH 7.0 with KOH. The extracellular solution for most experiments was ND-96 saline consisting of (mM): NaCl 96, KCl 2, $MgCl_2$ 1, $CaCl_2$ 1.8, HEPES 5, adjusted to pH 7.5 with NaOH. The extracellular sodium concentration was reduced in some experiments with ATX-II to achieve better voltage control by equimolar replacement of sodium with *N*-methyl-D-glucamine. Experiments were conducted at 21–24°C. To achieve rapid discharge of the membrane capacitance (<100 μs), we used agar bridges with Pt wires that had resistances <4 kohm and also used voltage measuring microelectrodes with resistances ≤0.5 Mohm when filled with 1 M KCl. Data were acquired using the program Pulse and most analyses were performed with the companion program Pulsefit (Instrutech Instruments, Great Neck, NY). Linear leak and capacity currents were subtracted by P/5 steps from −120 mV. Data were sampled at 50 kHz and filtered (f_c, −3db) at 10 kHz, unless otherwise indicated. A CA1 amplifier (Dagan Instruments) was also used for two microelectrode voltage clamp experiments. For these experiments, the current passing microelectrodes were filled with 0.7 M KCl plus 1.7 M K_3-citrate.

[1] *Abbreviations used in this paper:* ATX-II, toxin II from *Anemonia sulcata*; TTX, tetrodotoxin.

One limitation of our cut-open oocyte experiments was substantial accumulation of intracellular sodium, especially when ATX-II was used. This problem can be seen in Fig. 5 for Para/TipE sodium currents, where ATX-II caused a large change in reversal potential (E_{rev}). Sodium accumulation was a severe problem in this and similar experiments because there was no dialysis of the cytoplasm, the density of sodium channels was very high, and ATX-II dramatically increased the sodium influx. These problems were less severe in two-microelectrode voltage clamp experiments, where the density of sodium current was much lower. E_{rev} of toxin-modified channels in two-microelectrode experiments was +44.4 ± 2.5 mV (mean ± SEM, $n = 5$), a value similar to the most positive values obtained without toxin in cut-open oocyte experiments. ATX-II may cause a small change in E_{rev}, but the apparently large change seen in Fig. 5 is not due to a direct effect of toxin on sodium channel selectivity.

RESULTS

Construction of a Full Length para cDNA Clone

The complete *para* protein sequence was deduced from a series of six overlapping cDNA clones (Loughney et al., 1989; Ramaswami and Tanouye, 1989; Thackeray and Ganetzky, 1994). To facilitate expression studies of the *Drosophila para* sodium channel, we constructed a composite *para* cDNA clone as described in METHODS (Fig. 1 *A*). It has previously been shown that the *para* locus encodes a variety of different protein isoforms by alternative splicing (Loughney et al., 1989; Thackeray and Ganetzky, 1994). During our characterization of PCR amplification products derived from the *para* locus, we identified a new alternative exon. This optional exon is designated j, and is located in the presumptive amino-terminal cytoplasmic domain (Fig. 1 *A*). The *para* cDNA clone used in most of the present studies contains exons b, d, e, and lacks exons a and f and corresponds to the third most abundant combination of these alternative exons expressed in adults (Thackeray and Ganetzky, 1994).

The composite *para* cDNA clone encodes a sodium channel α subunit with a predicted molecular weight of 241 kD. To confirm that this cDNA encoded a full length *para* protein, it was expressed in an in vitro transcription/translation reaction. As shown in Fig. 1 *B*, this *para* cDNA clone encodes a protein of ~240 kD, consistent with its predicted molecular weight.

Heterologous Expression of para Sodium Channels in Xenopus Oocytes

Most mammalian homologs of *para* can be expressed in *Xenopus* oocytes as functional sodium channels, even though native channels contain additional subunits (Isom et al., 1994). However, we initially found no functional expression of *para* cRNA alone in *Xenopus* oocytes. Likewise, coexpression of *para* cRNA with the β_1 subunit of rat brain sodium channels did not encode functional sodium channels (data not shown).

In *Drosophila* embryonic neurons, functional sodium channels were found only in cells expressing Para isoforms containing exon a (O'Dowd et al., 1995*b*). Therefore, we also tested for expression of a second isoform of Para that contains exon a (called Para (a^+); this construct also contains exons b, d, e, j, and i, and lacks exon f); however, Para (a^+) also expressed poorly in our initial studies.

We next investigated whether other proteins are required for functional expression of *para* sodium channels. Classical genetic and biochemical analyses of the *tipE* locus suggested that this gene encodes a regulatory or structural component of *Drosophila* neuronal sodium channels (Ganetzky, 1986; Jackson, 1986). This locus was recently cloned (Feng et al., 1995*b*) and shown to encode a 50-kD acidic protein with two putative membrane spanning domains (Feng et al., 1995*a*). Indeed, coexpression of *para* and *tipE* cRNA in *Xenopus* oocytes produces robust expression of functional sodium channels, never seen in uninjected oocytes, water-injected oocytes, or oocytes injected with *tipE* cRNA alone (Fig. 2). Fig. 2 *A* shows superimposed current recordings for test potentials (V_t) ranging from −50 to +50 mV. These sodium channels activate and inactivate rapidly, with kinetics similar to those for native sodium channels in cultured *Drosophila* embryonic neurons (Byerly and Leung, 1988; O'Dowd and Aldrich, 1988; Saito and Wu, 1993). The corresponding current-voltage relationship is obtained by plotting the peak current vs. V_t (Fig. 2 *B*). This relationship is similar to that for mammalian sodium channels, except that the reversal potential is less positive. The reversal potential (+28 mV in this experiment) was highly variable (ranging from +12.8 to +44 mV in eight experiments), presumably reflecting variation in intracellular sodium concentration (see METHODS).

Fig. 2 *C* shows sodium currents at −10 mV elicited from various prepulse potentials (V_p) for the same oocyte. The corresponding voltage dependence of steady state inactivation is obtained by plotting the normalized peak inward current as a function of V_p (Fig. 2 *D*, ■). The solid curve is the best fit by a Boltzmann distribution and the midpoint and slope are similar to those for native *Drosophila* sodium channels. The data shown in Fig. 2 *B* was also used to evaluate the voltage dependence of activation. The relative sodium conductance (G_{Na}) is calculated assuming a linear current–voltage relationship (Fig. 2 *D*, □). The curve is the best fit by a Boltzmann distribution based on data for $V_t \leq +20$ mV.

Feng et al. (1995*a*) reported very small but reproducible sodium currents (50–200 nA) produced by injection of *para* cRNA alone into *Xenopus* oocytes. We find more robust expression of Para alone (currents >1 μA) when oocytes are injected with ≥50 ng of cRNA and incubated for at least 7 d at 18°C. The time and voltage

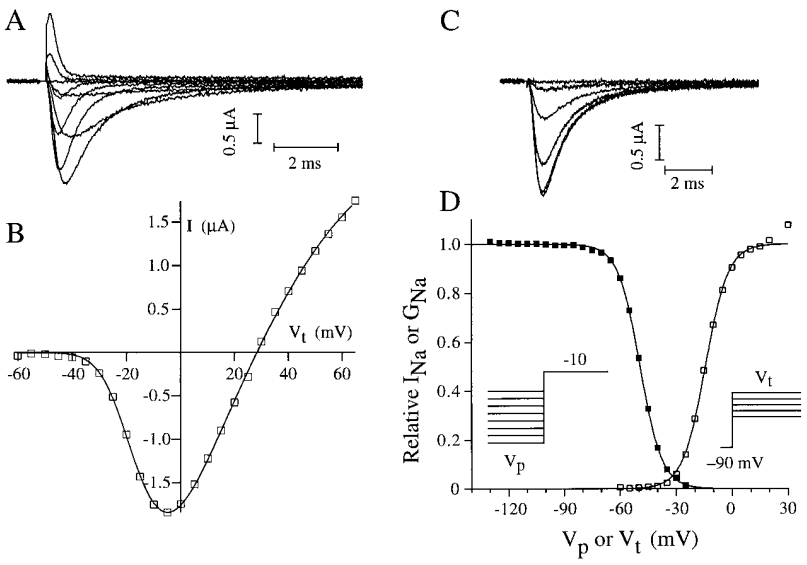

FIGURE 2. Voltage dependence of activation and inactivation of Para/TipE sodium channels expressed in a *Xenopus* oocyte. (*A*) Superimposed current records measured at test potentials (V_t) of −50, −30, −20, −10, +5, 15, 25, 35, and 50 mV from a holding potential of −90 mV. Blanking interval, 200 μs. (*B*) Peak sodium current plotted as a function of V_t. The reversal potential (+28 mV in this experiment) was highly variable, presumably reflecting variation in intracellular sodium concentration. Values up to +45 mV were observed. (*C*) Sodium currents measured at −10 mV from prepulse potentials (V_p) of −95, −70, −55, −45, −35, and −25 mV. Prepulse duration, 200 ms; blanking interval, 100 μs. (*D*) Voltage dependence of steady state availability and of activation of sodium current. Both sets of data are based on measurements of peak current during a test depolarization for the same experiment shown in the top panels. Both curves are the best fit by a Boltzmann distribution. The steady state availability data represents normalized measurements of peak inward current (■) and is plotted vs. V_p. The curve is defined by a slope factor = 5.89 mV, midpoint potential = −49.2 mV, and maximal current = 1.66 μA. The relative sodium conductance (G_{Na}) is calculated assuming a linear current–voltage relationship with a reversal potential of +28 mV (□). The curve is based on data for $V_t \leq +20$ mV; slope factor = 6.12 mV, midpoint potential = −14.3 mV, and maximal G_{Na} = 68.4 μS.

dependence of Para sodium currents is similar to that obtained when Para and TipE are coexpressed (Fig. 3). Since "old" oocytes are not well suited to the cut-open oocyte technique, Para sodium currents were measured only with a two-microelectrode voltage clamp. Consequently, changes in voltage were not as rapid as in the studies of Para/TipE shown in Fig. 2. Para/TipE sodium currents were measured with both voltage clamp

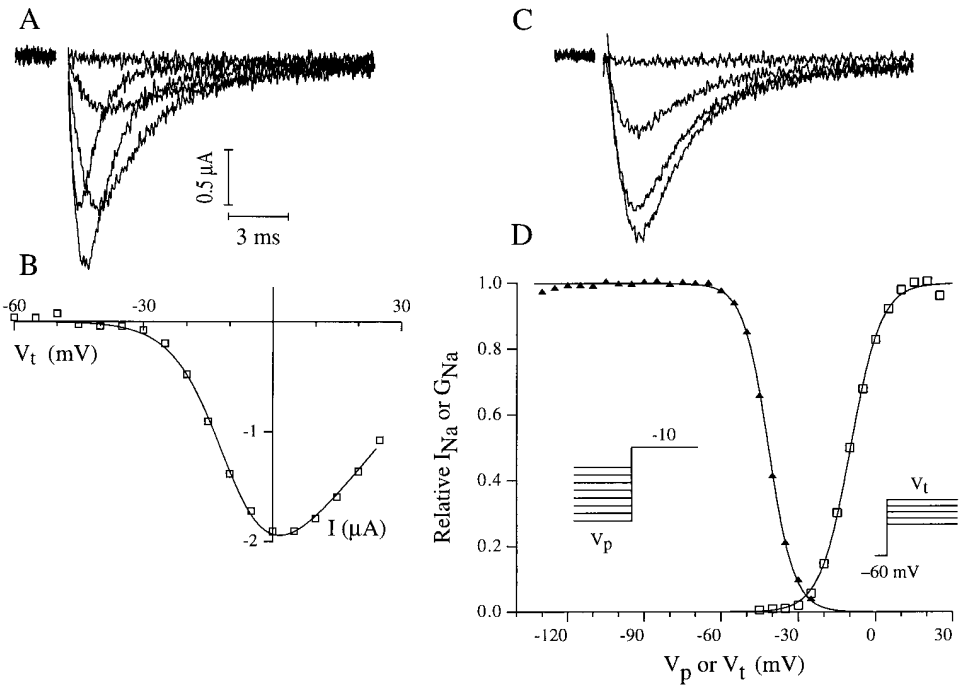

FIGURE 3. Voltage dependence of activation and of inactivation of Para sodium channels expressed in a *Xenopus* oocyte without TipE. (*A*) Superimposed current records measured at test potentials (V_t) of −35, −20, −10, +5, and 20 mV from a holding potential of −60 mV. Blanking interval, 640 μs. (*B*) Peak sodium current plotted as a function of V_t. The solid curve is the best fit by a Boltzmann distribution and linear current–voltage relationship, as described in (*D*). (*C*) Sodium currents measured at −10 mV from prepulse potentials (V_p) of −70, −50, −40, and −25 mV. Prepulse duration, 200 ms; blanking interval, 420 μs. (*D*) Voltage dependence of steady state availability and of activation of sodium current, determined in the same manner as for Fig. 2. Both curves are the best fit by a Boltzmann distribution. The steady state availability data represents normalized measurements of peak inward current (▲) and is plotted vs. V_p. The curve is defined by a slope factor = 4.77 mV, midpoint potential = −41.8 mV, and maximal current = 1.61 μA. The relative sodium conductance (G_{Na}) is calculated assuming a linear current–voltage relationship with a reversal potential of +48.7 mV (□). The curve is defined by a slope factor = 5.85 mV, midpoint potential = −9.8 mV, and maximal G_{Na} = 47.2 μS. All panels are for the same experiment using a two-microelectrode voltage clamp.

TABLE I

Effect of Exon a or TipE on the Voltage Dependence of Para Sodium Currents

Voltage clamp technique	Para/TipE		Para (a+)/TipE	Para
	Cut-open oocyte	Two μ-electrode	Two-microelectrode	Two-microelectrode
Activation				
$V_{1/2}$ (mV)	−15.8 ± 2.1	−16.9 ± 1.4	−16.8 ± 1.4	−12.2 ± 2.0
Slope factor (mV)	6.90 ± 0.41	5.43 ± 0.40	5.11 ± 0.21	5.58 ± 0.42
Number of experiments	9	10	4	6
Inactivation				
$V_{1/2}$ (mV)	−50.4 ± 1.2	−43.7 ± 0.7	−45.4 ± 0.6	−41.7 ± 1.0
Slope factor (mV)	6.09 ± 0.44	4.52 ± 0.14	4.26 ± 0.06	5.51 ± 0.63
Number of experiments	10	13	4	6

The voltage dependence of activation and inactivation were described by Boltzmann distributions; $V_{1/2}$ is the midpoint potential of the distribution. Each value is the mean±SEM.

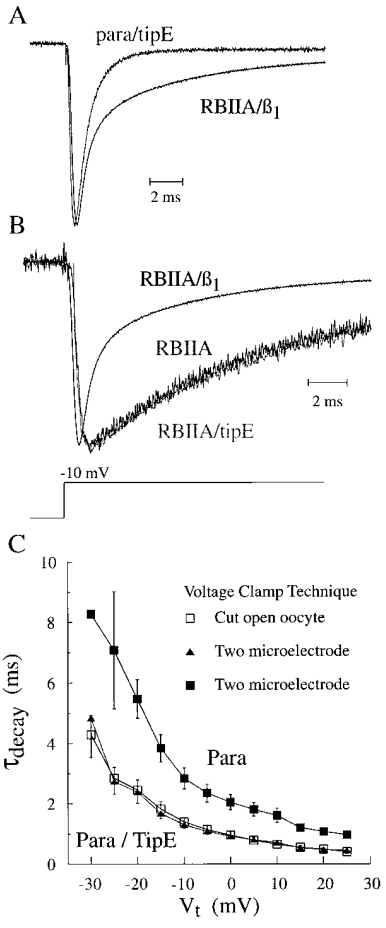

FIGURE 4. Para/TipE sodium channels inactivate more rapidly than rat brain IIA/β_1 or para sodium channels. (*A*) Coexpression of *para* and *tipE* results in sodium currents that inactivate rapidly, but coexpression of rat brain IIA α and β_1 results in sodium currents that inactivate with a biexponential time course. The amplitude of the slowly decaying component is fairly variable but typically ~30% of the peak inward current. Current records from two experiments are superimposed; the amplitude of the Para/TipE current is scaled up by 2.50. (*B*) TipE does not function as a β_1 subunit in association with a mammalian neuronal sodium channel. Current records from three experiments are superimposed with the amplitudes scaled so that peak inward currents are equal. The time course of sodium currents due to expression of RBIIA is unaffected by coexpression with TipE, but coexpression with β_1 results in much faster inactivation. Scale factors: 6.63 for RBIIA α; 5.89 for RBIIA α plus TipE. (*C*) Para sodium currents decay more rapidly when coexpressed with TipE. The time constant of decay of sodium current (τ_{decay}) is plotted as a function of V_t. The decay of each sodium current measurement was fit by a single exponential plus a constant. Each data point represents the mean of at least five experiments, except for two-microelectrode experiments with $V_t < -20$ mV. Para/TipE sodium currents were measured with both the cut-open (□) and two-microelectrode (▲) voltage clamp techniques. The error bars indicate the SEM. Only (−SEM) is indicated for two-microelectrode measurements and only (+SEM) is indicated for cut-open oocyte measurements. Para sodium currents were measured with only the two-microelectrode technique (■) and the error bars indicate ±SEM.

techniques to facilitate a comparison with Para sodium currents. A summary of this comparison is shown in Table I. The voltage dependence of activation and inactivation were described by Boltzmann distributions, as shown in Figs. 2 and 3. In general, there were no significant differences between the voltage dependencies measured with the two-microelectrode voltage clamp for Para/TipE vs. Para alone. Also, the two-microelectrode voltage clamp technique is a reliable measure of this voltage dependence because it gives results in good agreement with the cut-open oocyte technique.

TipE also enhanced the expression of Para (a^+) so that robust expression of this isoform was only observed when it was coexpressed with TipE (Fig. 3 and data not shown). Furthermore, there was little effect of exon a on the voltage dependence of activation or inactivation (see Table I).

TipE Modifies the Inactivation of Drosophila Sodium Channels

Mammalian neuronal and skeletal muscle sodium channel α subunits expressed in *Xenopus* oocytes function in two distinct gating modes: a slow and incompletely inactivating mode predominates, and a fast and completely inactivating mode is observed less frequently (Krafte et al., 1990; Moorman et al., 1990; Zhou et al., 1991; Fleig et al., 1994). Coexpression of a mammalian α subunit with a β_1 subunit in *Xenopus* oocytes increases the fraction of sodium channels gating in the fast mode (Makita et al., 1994; Patton et al., 1994). In contrast, Para/TipE sodium channels inactivate very rapidly without a homologous β_1 subunit (Fig.

4 *A*). This panel shows superimposed sodium currents measured during a depolarization to −10 mV. Note that all of the Para/TipE sodium channels inactivate rapidly, whereas a component of the RBIIA/β_1 sodium current inactivates slowly. The *tipE* protein exhibits no homology to mammalian sodium channel β subunits (Feng et al., 1995*a*). Fig. 4 *B* shows that TipE also does not substitute for a β_1 subunit. As previously reported, coexpression of the rat brain β_1 subunit with the RBIIA subunit results in much faster current inactivation (Patton et al., 1994). This effect of the β_1 subunit is one of the most dramatic effects of coexpression. However, the rate of inactivation of sodium current is unchanged when TipE is coexpressed with RBIIA. In contrast, coexpression of Para with TipE results in sodium currents that decay about twice as rapidly (Fig. 4 *C*). The decay of Para sodium currents is well fit by a single exponential, with or without coexpression of TipE. Fig. 4 *C* shows the time constant of decay (τ_{decay}) as a function of test potential. τ_{decay} for Para/TipE was the same with both voltage clamp techniques and was consistently faster than τ_{decay} for Para alone. This suggests that TipE is functioning like a β subunit of some sodium and potassium channels (see DISCUSSION).

Drosophila and Rat Brain IIA Channels Exhibit Distinct Pharmacological Properties

Sodium channels are a common target of animal and plant toxins (Adams and Olivera, 1994). A number of

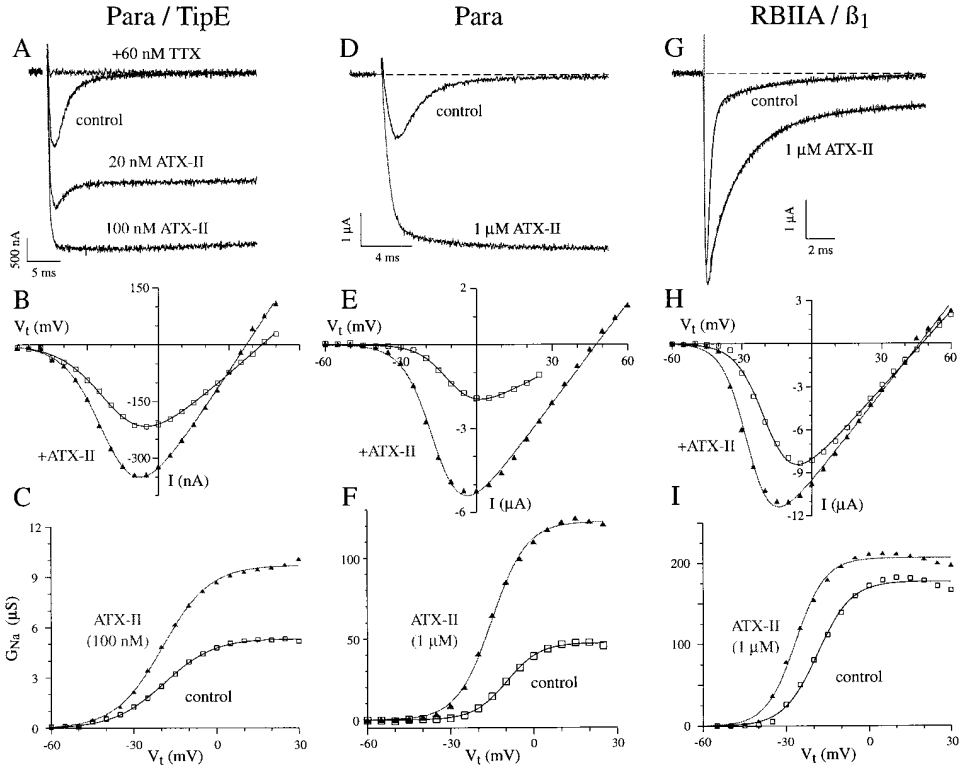

FIGURE 5. ATX-II slows the rate of inactivation of Para/TipE, Para, and rat brain IIA/β_1 sodium channels. (*Left column*) ATX-II greatly slows inactivation of Para/TipE sodium channels. (*A*) Sodium currents measured at −10 mV with and without 20 and 100 nM ATX-II and in 60 nM TTX. Sodium currents were measured with a two-microelectrode voltage clamp; holding potential, −45 mV; extracellular sodium, 20 mM; blanking interval, 660 µs. (*B*) Peak sodium current plotted as a function of V_t. Control, □; +100 nM ATX-II, ▲. Control reverse potential (E_{rev}) = +44.0 mV; E_{rev} = +37.3 mV in ATX-II. For *B*, *C*, *E*, *F*, *H* and *I*, control data is indicated by □, those in toxin are indicated by ▲, and the solid curves indicate the best fit by a Boltzmann distribution with a linear single channel current-voltage relationship. (*C*) Sodium conductance vs. V_t for the same experiment shown in (*B*). Note that ATX-II increases the maximal G_{Na} with little change in the voltage dependence of opening. Control Boltzmann distribution: slope factor = 9.32 mV, midpoint potential = −18.7 mV, maximal G_{Na} = 5.41 µS; +ATX-II: slope factor = 8.03 mV, midpoint potential = −20.2 mV, maximal G_{Na} = 9.44 µS. (*Center column*) ATX-II effects Para expressed without TipE in the same way as Para/TipE. (*D*) Sodium currents measured at 0 mV with and without 1 µM ATX-II. Note that the time to peak current in toxin is >10 ms, indicating that channel activation is not complete at the time of control peak inward current. Similar results were obtained with Para/TipE in 1 µM ATX-II. Blanking interval, 400 µs. (E) Peak sodium current plotted as a function of V_t. E_{rev} = +47.6 mV in ATX-II. E_{rev} = +48.7 mV for control assuming a linear single channel current–voltage relationship. (*F*) Sodium conductance vs. V_t for the same experiment shown in *D* and *E*. Control Boltzmann distribution: slope factor = 5.89 mV, midpoint potential = −9.8 mV, maximal G_{Na} = 47.2 µS; +ATX-II: slope factor = 6.31 mV, midpoint potential = −15.2 mV, maximal G_{Na} = 122.5 µS. (*Right column*) ATX-II slows inactivation of RBIIA/β_1 sodium channels to a lesser extent. (*G*) Sodium currents measured at +20 mV with and without 1.0 µM ATX-II. Each current record is fitted by the sum of two exponentials (with fast and slow time constants of decay, τ_f and τ_s) plus a constant. Control: τ_f = 0.289 ms; τ_s = 5.59 ms; +ATX-II: τ_f = 2.33 ms; τ_s = 30.78 ms. (*H*) Peak sodium current plotted as a function of V_t. E_{rev} = +47.3 mV for control; E_{rev} = +46.3 mV in ATX-II. (*I*) Sodium conductance vs. V_t for the same experiment shown in *H*. Note that ATX-II causes channel opening at more negative voltages with little change in maximal G_{Na}. Control Boltzmann distribution: slope factor = 6.11 mV, midpoint potential = −18.6 mV, maximal G_{Na} = 178 µS; +ATX-II: slope factor = 5.27 mV, midpoint potential = −26.6 mV, maximal G_{Na} = 206 µS.

commonly used insecticides also target sodium channels, but many cause toxicity that may be due to effects on vertebrate sodium channels (Vijverberg and van den Bercken, 1990; Bloomquist, 1993; Narahashi, 1996). Thus, it is desirable to compare the pharmacology of *Drosophila* sodium channels with that for a mammalian sodium channel, rat brain IIA. At least six distinct drug binding sites exist on this mammalian sodium channel (Catterall, 1992) and Figs. 5–8 show that Para sodium channels are more sensitive to ligands acting at three of these binding sites.

Toxin II from *Anemonia sulcata* slows the rate of inactivation of vertebrate and marine invertebrate sodium channels (Bergman et al., 1976; Norton, 1991). Modification of Para sodium channels by this toxin differs from that with other types of sodium channels in three principle ways: (*a*) the maximal sodium conductance ($G_{Na,max}$) is increased about twofold, but there is little or no increase in $G_{Na,max}$ for other types of sodium channels (alternatively, see Hanck and Sheets, 1995); (*b*) the time to peak current is greatly increased for Para channels; and (*c*) decay of Para sodium currents is slowed to a much greater extent than for other types of sodium channels. Fig. 5 shows the effects of ATX-II on Para sodium channels expressed with and without TipE (Fig. 5, *A–C* and *D–F*, respectively) and compares these

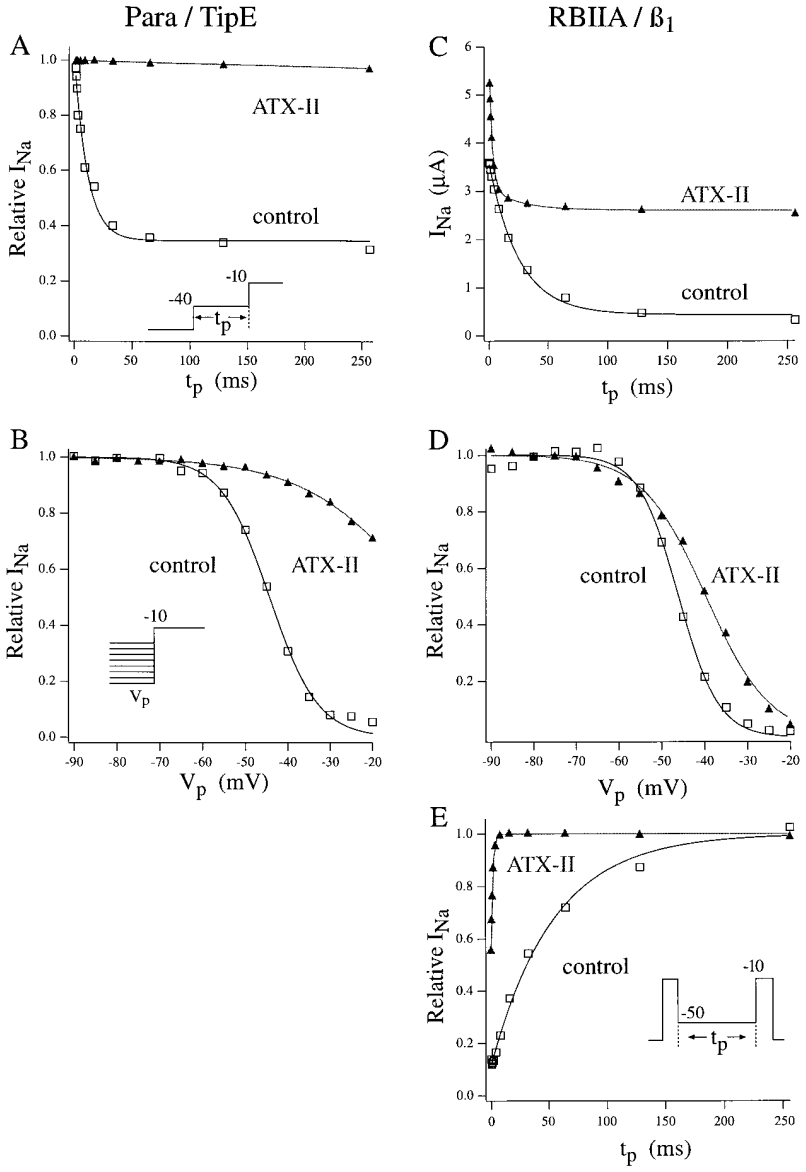

FIGURE 6. ATX-II modifies the onset and recovery from inactivation of Para/TipE and RBIIA/β_1 sodium channels. In all panels, open squares indicate control data, filled triangles indicate data in ATX-II, and measurements were made with a two-microelectrode voltage clamp. (*Left*) ATX-II slows inactivation of Para/TipE sodium channels during weak depolarizations that cause little channel activation. (*A*) Onset of inactivation at −40 mV with and without 500 nM ATX-II. The pulse protocol is indicated in the inset. The solid curves indicate the best fit to the equation: relative I_{Na} = $(A + Be(-t/\tau))/(A + B)$. Control, A = 504 nA, B = 908 nA, τ = 11.3 ms; +ATX-II, A = 0, B = 5.31 µA, τ = 9.5 s. (*B*) ATX-II modifies the availability of Para/TipE sodium channels. The normalized peak inward current is plotted vs. V_p. The solid curves indicate the best fit by a Boltzmann distribution. Control, I_{max} = 1.48 µA, midpoint potential = −44.3 mV, slope factor = 5.69 mV; +500 nM ATX-II: I_{max} = 5.52 µA, midpoint potential = −7.7 mV, slope factor = 13.7 mV; prepulse duration = 1 s. This prepulse duration is long enough for a steady state measurement in control, but not in ATX-II (see *A*). Same experiment as shown in *A*. (*Right*) Modification of onset and recovery from inactivation of RBIIA/β_1 sodium channels by ATX-II. (*C*) Onset of inactivation at −35 mV with and without 1 µM ATX-II. The solid curves indicate the best fit to $I_{Na} = A + B_{exp}(-t/\tau_1) + C_{exp}(-t/\tau_2)$. Control, A = 0.436 µA, B = 3.18 µA, τ_1 = 25.3 ms, C = 0; +ATX-II: A = 2.61 µA, B = 2.64 µA, τ_1 = 2.81 ms; C = 0.465 µA, τ_2 = 25.3 ms. Extracellular sodium, 20 mM. This result was typical of three experiments; the control rate of inactivation at −35 mV is 21.1 ± 2.6 ms; in 1 µM ATX -II, 18.3 ± 1.7% of the inactivating current decayed at the control rate and the rest decayed ~10-fold faster (a time constant of 2.34 ± 0.42 ms). (*D*) Normalized peak inward current vs. prepulse potential. Same pulse protocol as for *B*, same experiment as for *C*. The solid curves indicate the best fit by a Boltzmann distribution; control, I_{max} = 4.45 µA, midpoint potential = −46.1 mV, slope factor = 4.63 mV; +1 µM ATX-II: I_{max} = 7.20 µA, midpoint potential = −39.7 mV, slope factor = 7.46 mV. (*E*) ATX-II speeds the recovery from inactivation of RBIIA/β_1 sodium channels. The pulse protocol used is shown in the inset. The solid curves indicate the best fit to relative I_{Na} = $[A + B(1 - \exp(-t/\tau))]/(A + B)$. Control, A = 0.313 µA, B = 2.532 µA, τ = 53.7 ms; +2 µM ATX-II, A = 8.189 µA, B = 12.38 µA, τ = 1.61 ms.

effects with those on RBIIA/β_1 sodium channels (Fig. 5, *G–I*). ATX-II at 20 nM increases peak inward current and reduces rapid inactivation of Para/TipE sodium currents; at 100 nM, rapid inactivation is nearly eliminated and peak inward current is further increased. The current at the end of the depolarization was used to quantify the potency of toxin modification. This current was normalized by the current in maximally effective ATX-II (usually 1 μM toxin) and taken as the fraction of toxin-bound channels. This measure indicates that 20 nM toxin modifies about two-thirds of the channels (in two experiments, the modification was 51.5 and 68.7%). Assuming 1:1 binding, the dissociation constant (K_d) ≅ 10 nM. Fig. 5 *D* shows the maximal effect of ATX-II on Para sodium channels. Note that slowing inactivation with ATX-II results in a current that reaches a maximum much later, suggesting that channel activation is relatively slow and not complete at the time of control peak current. Similar results were obtained with 1 μM ATX-II with either Para/TipE or Para (a^+)/TipE (data not shown).

ATX-II also slows inactivation of RBIIA/β_1 sodium channels, but to a lesser extent than for Para (Fig. 5 *G*). The decay of RBIIA/β_1 sodium currents with and without 1 μM ATX-II is fit by the sum of two exponentials. Both components of current decay are slowed by ATX-II, indicating that all channels are modified by 1 μM toxin. However, the degree of slowing of inactivation (5–10-fold increase in each time constant) is much less than for Para/TipE or for Para alone. The time constant for decay of Para/TipE sodium currents in 1 μM ATX-II is >3 s at 0 mV, indicating a slowing of at least 1,000-fold (data not shown). Although the binding affinity of ATX-II to some mammalian sodium channels is comparable in potency with that for Para/TipE (K_d ≅ 10 nM), the toxin causes a 100-fold greater decrease in the rate of inactivation of Para/TipE; therefore, the toxin should have a much greater effect on sodium influx through *Drosophila* sodium channels.

ATX-II (1 μM) increases the peak inward current of RBIIA/β_1 sodium channels for weak but not for strong depolarizations (Fig. 5 *H*). The solid curves indicate the best fit by a Boltzmann distribution assuming a linear single channel current–voltage relationship. These data are converted into conductance measurements and plotted to illustrate more clearly that ATX-II shifts the voltage dependence of RBIIA/β_1 channel opening to more negative voltages, but has little effect on maximal conductance (Fig. 5 *I*). In contrast, ATX-II increases the maximal conductance of Para/TipE or Para sodium currents, with little effect on the voltage depen-

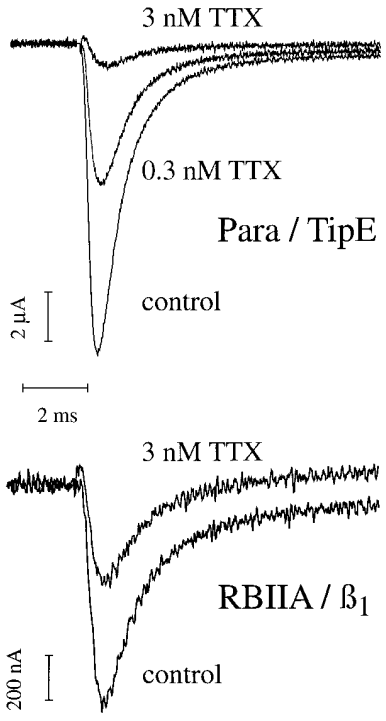

FIGURE 7. Tetrodotoxin block of Para/TipE and rat brain IIA/β_1 sodium channels. (*Top*) Superimposed Para/TipE sodium currents measured at −10 mV with 0, 0.3, and 3.0 nM TTX. Blanking interval, 100 μs. (*Bottom*), Superimposed RBIIA/β_1 sodium currents measured at −10 mV in 0 and 3 nM TTX. No blanking interval.

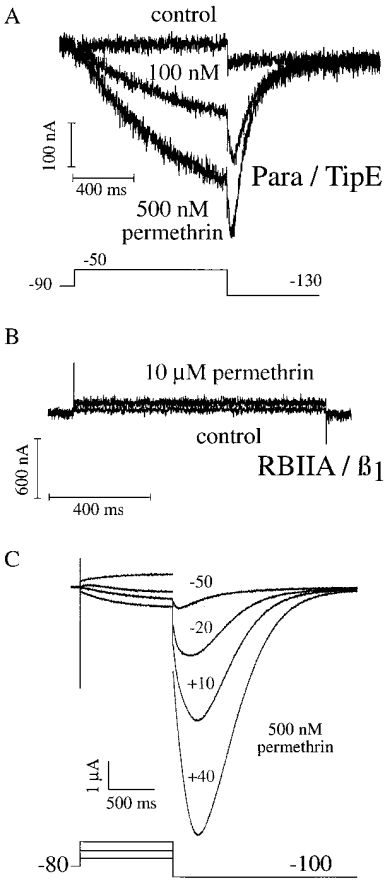

FIGURE 8. Permethrin effects on Para/TipE and rat brain IIA/β_1 sodium channels. Sodium currents were measured using a two-microelectrode voltage clamp for both experiments shown in this figure. (*A*) Permethrin causes opening of Para/TipE sodium channels during long depolarizations to −50 mV. The current deactivates slowly when the membrane is repolarized to −130 mV, with a rising phase, or hook, on the tail currents. Maximal peak inward current (at V_t = −15 mV), 3.2 μA; sampling interval, 1.0 ms. (*B*) 10 μM permethrin does not have a similar effect on RBIIA/β_1 sodium channels. No effects were seen at other test potentials. Maximal peak inward current (at V_t = −5 mV), 4.43 μA. (*C*) Modification of Para/TipE by 500 nM permethrin increases with test pulse voltage. Same experiment as shown in *A*. Depolarizations to the indicated voltages elicited currents that activated and inactivated rapidly, as for control, followed by slowly activating currents that were seen only with permethrin. The rapidly inactivating currents are not accurately measured with the sampling interval of 1.0 ms used for this experiment.

dence of channel activation. For Para/TipE sodium currents, ATX-II increased $G_{Na,max}$ by a factor of 1.96 ± 0.69 and $V_{1/2}$ was shifted −3.2 ± 5.8 mV (n = 7). Likewise, $G_{Na,max}$ for Para expressed alone was increased by a factor of 2.53 and $V_{1/2}$ was shifted −2.5 ± 3.3 mV (n = 2). Although the effect of ATX-II on these mammalian and insect sodium channels appears quite dissimilar, both actions can be accounted for by slowing of inactivation (see DISCUSSION).

ATX-II and anthopleurin A, a sea anemone toxin that is structurally and functionally similar to ATX-II, slow inactivation of cardiac sodium channels from open states, but not from closed states (El-Sherif et al., 1992; Hanck and Sheets, 1995). Toxin IV-5 from the scorpion *Tityus serrulatus*, which acts at the same site on sodium channels as ATX-II, also selectively modifies inactivation from open states in studies with neuronal sodium channels (Kirsch et al., 1989). Inactivation from closed states is most significant for weak depolarizations that cause a substantial amount of inactivation but very little channel opening. For Para/TipE sodium channels, the voltage range where these conditions exist is from −55 to −40 mV (see Fig. 2 *D* and Table I). Fig. 6, *A* and *B* shows that ATX-II slows inactivation even during depolarizations that cause activation of <1% of the sodium channels. The rate of onset of inactivation at −40 mV was determined by varying the duration of a conditioning prepulse (Fig. 6 *A*, *inset*). The solid curve through the control data is the best fit by a single exponential and indicates a time constant of 11.3 ms. This result is representative of six experiments in which the time constant of inactivation at −40 mV was 13.9 ± 1.6 ms. In ATX-II, the rate of inactivation is ~1,000-fold slower (the best-fit time constant is 9.5 s, but the rate is not well defined). Similar results were obtained in three experiments with Para/TipE and in one experiment when Para was expressed without TipE.

ATX-II also slows the development of inactivation at more negative voltages (Fig. 6 *B*). The voltage dependence of inactivation was determined using the pulse protocol shown in the inset with a prepulse duration (t_p) of 1 s. Very little inactivation occurred for prepulses to voltages ≤−40 mV. Thus, ATX-II causes a dramatic slowing of inactivation over a broad voltage range, in contrast with the effects of sea anemone toxins on mammalian cardiac sodium channels. This indicates that inactivation from closed states is unimportant for Para/TipE sodium channels or that ATX-II slows inactivation from both closed and open states for these channels.

Similar experiments with RBIIA/β_1 sodium channels indicate a much more complicated effect of toxin. Fig. 6 *C* shows the effects of ATX-II on the rate of onset of inactivation at −35 mV. The control data (□) is well fit by a single exponential plus a constant. In 1 μM ATX-II, the time course of inactivation is better fit by the sum of two exponentials plus a constant. Although toxin slows inactivation during strong depolarizations (Fig. 5 *G*), it speeds inactivation of a component of current during weak depolarizations. The slower exponential component in toxin decays with the same time constant as for control, suggesting that toxin modification is incomplete. In addition, the noninactivating current is increased by ATX-II. Similar effects were seen at more negative voltages, although the second exponential component, corresponding to unmodified channels, was usually smaller than at −35 mV. A small speeding of inactivation by sea anemone toxins has been reported for cardiac sodium channels (Hanck and Sheets, 1995), but the dramatic effect seen in Fig. 6 *C* is unexpected and is not accounted for by previous models of toxin action.

The main effect of ATX-II on the steady state availability of RBIIA/β_1 sodium channels is to reduce the slope factor (Fig. 6 *D*). The solid curves indicate the best fit by a Boltzmann distribution. The control distribution was defined by midpoint potential = −52.6 ± 3.4 mV, slope factor = 4.55 ± 0.11 mV (n = 3); in these cells, after adding 1 μM ATX-II, the distribution was: midpoint potential = −42.8 ± 2.1 mV, slope factor = 7.97 ± 0.29 mV. As expected from previous studies with muscle sodium channels (Chahine et al., 1996), ATX-II also accelerates the rate of recovery from inactivation (Fig. 6 *E*). The recovery from inactivation was described by a single exponential at −50 mV with a time constant of 35.2 ± 9.2 ms (n = 3). In 1 μM ATX-II, the recovery was fit by an exponential plus a constant, with a time constant of 1.79 ± 0.1 ms (n = 3). This result indicates that ATX-II destabilizes the inactivated state.

Tetrodotoxin (TTX)[1] is one of the most commonly used sodium channel ligands because it selectively blocks most neuronal and skeletal muscle sodium channels with a dissociation constant of 1–10 nM (Ritchie and Rogart, 1977; Catterall, 1980). TTX block of endogenous sodium channels in *Xenopus* oocytes has been quantified so that studies with this toxin can confirm the expression of heterologous channels (see DISCUSSION). Block of Para/TipE sodium channels is ~10-fold more potent than for RBIIA/β_1 sodium channels (Fig. 7), as predicted by earlier ligand binding studies (Pauron et al., 1985) and as reported for Para/TipE (Feng et al., 1995*a*). Fig. 7, *upper panel* shows that 0.3 nM TTX blocks approximately half of the sodium current and 3 nM toxin causes almost complete block. This result is representative of four experiments in which 0.3 nM TTX blocked 50.5 ± 7.0% (±SEM) of the peak sodium current. Similar results are obtained when Para is expressed alone (data not shown). In contrast, 3 nM TTX causes only half-maximal block of RBIIA/β_1 (Fig. 7, *lower panel*), consistent with earlier reports with RBII or RBIIA alone (Terlau et al., 1991; Kontis and Goldin, 1993).

Pyrethroids, such as permethrin, modify sodium channels, causing them to open at inappropriate times and voltages, resulting in repetitive firing of neuronal action potentials followed by conduction block, paralysis, and death (Vijverberg and van den Bercken, 1990; Bloomquist, 1993; Narahashi, 1996). Permethrin is at least 100-fold more potent on the Para/TipE sodium channel than on the mammalian RBIIA/β_1 sodium channel (Fig. 8, *A* and *B*). Note that 100 nM permethrin causes substantial opening of Para/TipE sodium channels during the depolarization to −50 mV, and also slows channel closing when the membrane is repolarized to −130 mV. A voltage near the foot of the activation curve (−50 mV) was chosen for demonstrating the effects of permethrin because only drug-modified channels open at this voltage. Permethrin at 500 nM causes greater modification with little change in the time course of the drug-modified current. In contrast, 10 μM permethrin has no effect on RBIIA/β_1 sodium channels under equivalent conditions (Fig. 8 *B*).

Modification of Para/TipE sodium channels by permethrin was enhanced by stronger depolarizations (Fig. 8 *C*). Permethrin at 500 nM causes a slowly activating current at all test potentials, and the tail current after repolarization increases with test potential, indicating increased permethrin modification. The rapidly inactivating sodium current seen in control is little affected by permethrin, but is not well resolved at the slow sampling rate used in this study. The drug-induced tail current has been used to quantify pyrethroid modification of vertebrate sodium channels (Vijverberg et al., 1983; Song and Narahashi, 1996). Permethrin-induced tail currents for Para/TipE decay at least 100-fold more slowly than those observed in studies of mammalian or marine invertebrate sodium channels. This indicates that insect sodium channels will remain open for a much longer time after an action potential and the drug effect on electrical activity will be enhanced (see DISCUSSION). Also note that the permethrin-induced tail current increases when the test potential is increased from +10 to +40 mV, a voltage range where activation and inactivation are maximal. This suggests that the voltage dependence of drug modification cannot be easily attributed to preferential binding to open or inactivated channels. Finally, the tail current has a more prominent rising phase or "hook" as the preceding test pulse becomes more positive. This change in time course greatly complicates quantification of permethrin effects because the simplest schemes predict that the time course does not change with the fraction of modified channels (Zong et al., 1992). Modification by permethrin of RBIIA/β_1 over this same voltage range is at least 100-fold less potent then for Para/TipE (data not shown).

DISCUSSION

Para is the first invertebrate sodium channel to be heterologously expressed in *Xenopus* oocytes (see also Feng et al., 1995*a*). Our results demonstrate that robust functional expression is facilitated by coexpression with TipE, a protein that lacks homology with any known subunit of mammalian sodium channels. Coexpression of *para* and *tipE* appears to reconstitute all the biophysical and pharmacological properties of native sodium channels recorded from cultured *Drosophila* embryonic neurons. Previous experiments have shown that *para* encodes the predominant sodium channel isoforms expressed in embryos and larvae (Hong and Ganetzky, 1994). Analyses of Para sodium channels expressed in *Xenopus* oocytes and sodium currents expressed in embryonic neurons reveal that both exhibit: (*a*) channel activation by depolarizing test pulses to ∼−35 mV; (*b*) maximum peak current at a test pulse between −20 and −5 mV; (*c*) complete inactivation of the inward current within 5 ms; and (*d*) complete block of the inward current by 10 nM TTX (Byerly and Leung, 1988; O'Dowd and Aldrich, 1988; Baden, 1989; Saito and Wu, 1993). Taken together, these observations suggest that coexpression of *para* and *tipE* reconstitute the native Para sodium channel.

It is unlikely that the observed sodium current is due to upregulation of an endogenous sodium channel since it was observed only in oocytes that were injected with *para*, but never in uninjected oocytes, water-injected oocytes, or oocytes injected with only *tipE* (data not shown). While it has been reported that ∼5% of *Xenopus* oocytes exhibit a small endogenous voltage-activated sodium current (270 ± 17 nA) (Krafte and Volberg, 1992), >90% of the oocytes injected with *para* and *tipE* exhibit robust sodium currents with peak current amplitudes >1 μA. In addition, the steady state inactivation of the endogenous oocyte sodium current is half-maximal at −38 ± 0.5 mV, while the half-maximal steady state inactivation of the Para/TipE sodium channel is −44.3 ± 0.9 mV (Table I), and the IC_{50} for TTX block of the endogenous sodium channel is 6 nM, while the IC_{50} for TXX block of the Para/TipE sodium channel is ∼0.3 nM (Fig. 7). Together, these results confirm that the observed sodium current is indeed the result of heterologous coexpression of *para* and *tipE*.

What is the nature of the interaction between the *para* and *tipE* proteins that facilitates expression of functional sodium channels? Given that *tipE* appears to encode a novel transmembrane protein with two membrane spanning domains, it is appealing to speculate that TipE is a novel sodium channel accessory protein (Feng et al., 1995*a*). Indeed, TipE enhances expression of Para, in a manner analogous to that of β subunits of mammalian neuronal and cardiac sodium channels,

muscle calcium channels, *Drosophila Shaker* potassium channels, and mammalian *Shaker*-related potassium channels (Isom et al., 1994; Rettig et al., 1994; Chouinard et al., 1995; McManus et al., 1995; Qu et al., 1995). Furthermore, TipE causes a speeding of current decay, reminiscent of the effect of other sodium and potassium channel β subunits (Isom et al., 1994; Makita et al., 1994; Patton et al., 1994; Rettig et al., 1994; Chouinard et al., 1995). Although the β subunits for voltage-gated ion channels have some similar biophysical effects, they are structurally diverse. The predicted secondary structure and membrane topology of TipE are similar to that predicted for the β subunit of calcium-activated potassium channels (Knaus et al., 1994). However, *TipE* has little primary amino acid sequence similarity to any known protein, and β subunits of mammalian sodium channels have one membrane spanning domain, but TipE has two. As an alternative, it is possible that TipE may play a role in regulating the expression or posttranslational processing of Para. Therefore, future studies aimed at determining how TipE affects the expression of Para and at determining if Para and TipE coassemble in the extracellular membrane will be required to determine the exact nature of the *para–tipE* interaction. In addition, we have examined only 2 of over 100 possible Para isoforms encoded by alternative splicing, and it is possible that an alternative isoform may encode sodium channels with different biophysical and pharmacological properties, as well as isoforms that may not be as dependent on coexpression with TipE.

Based on single cell PCR after electrophysiological analysis, O'Dowd et al. (1995) concluded that exon a (Fig. 1 *A*) is necessary but not sufficient for expression of functional sodium currents in embryonic neurons. However, we found that TipE was also required for robust expression of Para (a^+) and that channel gating is very similar for Para isoforms with and without exon a (see Table I). Moreover, ~30% of the *para* mRNAs in embryos lack exon a, as do approximately half of the *para* mRNAs in adults (Thackeray and Ganetzky, 1994). O'Dowd et al. (1995) proposed that transcripts excluding exon a might encode: (*a*) proteins that fail to encode functional channels, (*b*) channels with novel gating properties or, (*c*) functional channels that are localized to membrane sites electrically separated from the cell body. Our results rule out the first two possibilities and suggest either that transcripts lacking exon a are localized to membrane sites such as distal processes or synapses that are not detected in the cultured embryonic neurons, or that transcripts lacking exon a require developmental cues for expression that are absent in cultured neurons.

We have compared the pharmacology of the *Drosophila* Para/TipE and RBIIA/β_1 sodium channels at three distinct toxin binding sites and found that the Para/TipE sodium channel is more sensitive to all three toxins that we tested. ATX-II is a peptide toxin that binds to the α-scorpion toxin binding site on sodium channels (Norton, 1991). This toxin affects only inactivation of mammalian neuronal and muscle sodium channels (Kirsch et al., 1989; El-Sherif et al., 1992; Cannon and Corey, 1993; Hanck and Sheets, 1995) and probably acts in the same way on Para/TipE channels. Rapid inactivation of Para/TipE sodium channels is nearly eliminated by ATX-II with an $ED_{50} \cong 10$ nM (Fig. 5). Binding with similar potency has been reported for heterologously expressed mammalian RBIIA and muscle sodium channels (Chahine et al., 1996; Rogers et al., 1996), but some studies with native channels indicate much weaker binding (Bergman et al., 1976; El-Sherif et al., 1992; Cannon and Corey, 1993). Thus, ATX-II is insect selective not because it binds with greater affinity to insect sodium channels, but because it produces a much more profound slowing of channel inactivation over a broader voltage range. The time constant describing current decay (τ_{decay}) of toxin-modified mammalian muscle sodium currents is 10–30 ms (El-Sherif et al., 1992; Chahine et al., 1996), and we find similar slowing of RBIIA/β_1 sodium currents (see Fig. 5). In contrast, $\tau_{decay} > 3$ s for Para/TipE.

For Para/TipE, ATX-II increases $G_{Na,max} \cong$ twofold, prolongs the time to peak current, and has little effect on the apparent voltage dependence of activation (Fig. 5). In contrast, $G_{Na,max}$ is little changed for RBIIA/β1 channels, there is a much smaller increase in time to peak current, and activation is shifted to more negative voltages. Although the effects of ATX-II on Para/TipE and RBIIA/β_1 sodium channels appear quite dissimilar, the actions can be accounted for solely by slowing of inactivation. The effects of ATX-II on RBIIA/β_1 channels are similar to those of other inhibitors of inactivation on neuronal sodium channels (Gonoi and Hille, 1987) and can be accounted for if RBIIA/β_1 channels must open before inactivating. The shift in voltage dependence of activation occurs because the rate of inactivation is comparable to the rate of opening for weak depolarizations, but much slower than the rate of opening for strong depolarizations (Gonoi and Hille, 1987). Thus, sodium currents are increased by toxin modification for weak but not for strong depolarizations. By analogy, the effects of ATX-II on Para/TipE suggest that the overlap between activation and inactivation is similar at all voltages (as for cardiac sodium channels; see Hanck and Sheets, 1995), and channel activation is relatively slow and not complete at the time of control peak current. The large increase in $G_{Na,max}$ suggests that ATX-II also inhibits inactivation from closed states and that many Para channels normally inactivate without first opening.

Studies of inactivation using conditioning prepulses of varying duration also suggest that ATX-II inhibits in-

activation from closed states of Para/TipE sodium channels (Fig. 6). Inactivation from closed states is most significant at voltages corresponding to the foot of the activation curve and ATX-II is equally effective at slowing inactivation at these voltages as at more positive potentials. The effects of ATX-II on Para/TipE sodium channels are very similar to the effects of changing residues 1488–1490 of RBIIA/β_1 sodium channels to glutamine (West et al., 1992); in both cases, the rate of inactivation is slowed ~1,000-fold with little change in the voltage dependence of activation. This suggests that the mutation slows inactivation from both closed and open states. Surprisingly, the effects of ATX-II on RBIIA/β_1 sodium channels are different from elimination of inactivation by this mutation (Figs. 5 and 6). ATX-II slows inactivation of RBIIA/β_1 sodium current during strong depolarizations, but has a mixed effect during weak depolarizations; fewer channels inactivate, but those that inactivate do so more rapidly than normal (Fig. 6 *C*). This suggests that, as for cardiac sodium channels, ATX-II does not slow inactivation of RBIIA/β_1 channels from closed states. Toxin effects on RBIIA sodium channels expressed in oocytes are particularly complex because these channels can enter a slow gating mode that causes a noninactivating current (Fleig et al., 1994). It is possible that ATX-II also affects transitions into this slow gating mode.

Pyrethroids are highly toxic to insects, but have low mammalian toxicity. Previous studies indicated that the insect specificity of pyrethroid action is due primarily to three factors (Song and Narahashi, 1996): (*a*) pyrethroids increase in potency as the temperature decreases and act in insects at lower temperatures; (*b*) pyrethroids bind to invertebrate sodium channels with greater affinity than to mammalian sodium channels; and (*c*) pyrethroids are detoxified more effectively in mammals. Previous voltage clamp studies have used marine invertebrate sodium channels as a surrogate for insect sodium channels. These studies indicate that the threshold concentration of tetramethrin necessary to produce abnormal electrical spiking activity in marine invertebrate neurons is ~10-fold lower than for mammalian neurons with TTX-sensitive sodium channels (Song and Narahashi, 1996). However, the TTX-resistant sodium channels found in mammalian dorsal root ganglion neurons are 30–100-fold more sensitive to pyrethroids than TTX-sensitive sodium channels (Tatebayashi and Narahashi, 1994), so some mammalian sodium channels are as sensitive to pyrethroids as previously studied marine invertebrate channels. Our results show that the Para/TipE sodium channel is at least 100-fold more sensitive to the pyrethroid permethrin than the RBIIA/β_1 sodium channel, and demonstrate that selective binding to insect sodium channels is a major determinant of the selective toxicity of pyrethroid insecticides.

The most potent effects of pyrethroids are to induce repetitive afterdischarges after a single stimulus. This action requires that sodium channels remain open after an action potential and that the inward currents reach threshold levels needed to trigger an extra action potential. Permethrin-induced tail currents for Para/TipE decay at least 100-fold more slowly than those observed in studies of vertebrate sodium channels (Vijverberg et al., 1983). Thus, modified insect sodium channels will remain open for a much longer time after an action potential and the modification produced by each action potential can more readily summate to threshold levels. Both pyrethroids and ATX-II enhance channel opening by slowing transitions out of the open state; both toxins have a more extreme effect on insect sodium channels than on mammalian sodium channels, resulting in insect-specific drug action.

Taken together, our results show that the basic biophysical properties of the insect and mammalian sodium channels examined in this study are similar, but the Para/TipE sodium channels are much more sensitive to all of the toxins that we have studied. The functional expression of *Drosophila* Para sodium channels and unique pharmacology of this channel facilitates an analysis of the relationship between channel structure and function. One can now determine the nature of the *para–tipE* interaction, can evaluate the functional consequences of the different Para isoforms encoded by alternative splicing, and can map specific neurotoxin and insecticide binding sites. These studies will provide new insights into the mechanisms underlying sodium channel diversity and insecticide resistance.

We thank Guoping Feng, Peter Deak, and Linda M. Hall (SUNY-Buffalo) for providing unpublished data on the *tipE* gene and their *para/tipE* coexpression studies, and thank Maninder Chopra and Dejian Ren (SUNY-Buffalo) for providing the *tipE* RNA used in our initial expression studies. Plasmid vectors encoding the rat brain IIA α subunit (Zem-RVSP6-2580) and rat brain β_1 subunit (p β_1.c1Aa) were obtained from Lori L. Isom and William A. Catterall (University of Washington), and the pGH19 vector was provided by Evan Goulding and Steven Siegelbaum (Columbia University). We thank Paul Liberator and Jennifer Anderson for producing some synthetic oligonucleotides and Richard Brochu for preparing some of the oocytes.

This work was supported in part by a National Institutes of Health Postdoctoral Fellowship to R. Reenan and by grants from the Markey Charitable Trust, Merck Research Laboratories, and National Institutes of Health (GM-43100) and a Klingenstein fellowship to B. Ganetzky. This is paper 3464 from the Laboratory of Genetics, University of Wisconsin, Madison.

Original version received 30 December 1996 and accepted version received 14 May 1997.

REFERENCES

Adams, M.E. and M. Olivera. 1994. Neurotoxins: overview of an emerging research technology. *Trends Neurosci.* 17:151–155.

Arena, J.P., K.K. Liu, P.S. Paress, and D.F. Cully. 1991. Avermectin-sensitive chloride currents incuded by *Caenorhabditis elegans* RNA in *Xenopus* oocytes. *Mol. Pharmacol.* 40:368–374.

Arena, J.P., K.K. Liu, P.S. Paress, J.M. Schaeffer, and D.F. Cully. 1992. Expression of a glutamate-activated chloride current in Xenopus oocytes injected with Caenorhabditis elegans RNA: evidence for modulation with avermectin. *Mol. Brain Res.* 15:339–348.

Baden, D.G. 1989. Brevetoxins: unique polyether dinoflagellate toxins. *FASEB J.* 3:1807–1817.

Bergman, C., J.M. Dubois, E. Rojas, and W. Rathmayer. 1976. Decreased rate of sodium conductance inactivation in the node of Ranvier induced by a polypeptide toxin from sea anemone. *Biochim. Biophys. Acta.* 455:173–184.

Bloomquist, J.R. 1993. Neuroreceptor mechanisms in pyrethroid mode of action and resistance. *In* Reviews in Pesticide Toxicology. R.M. Roe and R.J. Kuhr, editors. Toxicology Communications Inc., Raleigh, NC. 185–230.

Byerly, L., and H.T. Leung. 1988. Ionic currents of Drosophila neurons in embryonic cultures. *J. Neurosci.* 8:4379–4393.

Cannon, S.C., and D.P. Corey. 1993. Loss of Na^+ channel inactivation by anemone toxin (ATX II) mimics the myotonic state in hyperkalaemic periodic paralysis. *J. Physiol. (Camb.).* 466:501–520.

Catterall, W.A. 1980. Neurotoxins that act on voltage-sensitive sodium channels in excitable membranes. *Annu. Rev. Pharmacol. Toxicol.* 20:14–43.

Catterall, W.A. 1992. Cellular and molecular biology of voltage-gated sodium channels. *Physiol. Rev.* 72:S15–S48.

Chahine, M., E. Plante, and R.G. Kallen. 1996. Sea anemone toxin (ATX II) modulation of heart and skeletal muscle sodium channel α-subunits expressed in tsA201 cells. *J. Membr. Biol.* 152:39–48.

Chouinard, S.W., G.F. Wilson, A.K. Schlimgen, and B. Ganetzky. 1995. A potassium channel β subunit related to the aldo-keto reductase superfamily is encoded by the *Drosophila* hyperkinetic locus. *Proc. Natl. Acad. Sci. USA.* 92:6763–6767.

Dong, K., and J.G. Scott. 1994. Linkage of *kdr*-type resistance and the *para*-homologous sodium channel gene in German cockroaches (*Blattella germanica*). *Insect Biochem. Mol. Biol.* 24:647–654.

El-Sherif, N., H.A. Fozzard, and D.A. Hanck. 1992. Dose-dependent modulation of the cardiac sodium channel by sea anemone toxin ATXII. *Circ. Res.* 70:285–301.

Ertel, E.A., T.A. Bale, and C.J. Cohen. 1994. Modification of insect neuronal Na and Ca channels by deltamethrin. *Soc. Neurosci. Abstr.* 20:717.

Feng, G., P. Deak, M. Chopra, and L.M. Hall. 1995*a*. Cloning and functional analysis of *TipE*: a novel membrane protein which enhances Drosophila *para* sodium channel function. *Cell.* 82:1001–1011.

Feng, G., P. Deak, D.P. Kasbekar, D.W. Gil, and L.M. Hall. 1995*b*. Cytogenetic and molecular localization of tipE: a gene affecting sodium channels in Drosophila melanogaster. *Genetics.* 139: 1679–1688.

Fleig, A., P.C. Ruben, and M.D. Rayner. 1994. Kinetic mode switch of rat brain IIA Na channels in *Xenopus* oocytes excised macropatches. *Pflugers Arch.* 427:399–405.

Ganetzky, B. 1986. Neurogenetic analysis of Drosophila mutations affecting sodium channels: synergistic effects on viability and nerve conduction in double mutants involving *tip-E*. *J. Neurogen.* 3:19–31.

Goldin, A.L. 1992. Maintenance of *Xenopus laevis* and oocyte injection. *In* Methods in Enzymology. B. Rudy and L.E. Iverson, editors. Academic Press, Inc., New York. 266–278.

Gonoi, T., and B. Hille. 1987. Gating of Na channels: inactivation modifiers discriminate among models. *J. Gen. Physiol.* 89:253–274.

Guy, H.R., and F. Conti. 1990. Pursuing the structure and function of voltage-gated channels. *Trends Neurosci.* 13:201–206.

Hall, L.M., and D.R. Kasbekar. 1989. Drosophila sodium channel mutations affect pyrethroid sensitivity. *In* Insecticide Action from Molecule to Organism. T. Narahashi and J.E. Chambers, editors. Plenum Press, New York. 99–114.

Hanck, D.A., and M.F. Sheets. 1995. Modification of inactivation in cardiac sodium channels: ionic current studies with anthopleurin-A toxin. *J. Gen. Physiol.* 106:601–616.

Hodgkin, A.L., and A.F. Huxley. 1952. Currents carried by sodium and potassium ions through the membrane of the giant axon of Loligo. *J. Physiol. (Camb.).* 116:449–472.

Hong, C.S., and B. Ganetzky. 1994. Spatial and temporal expression patterns of two sodium channel genes in Drosophila. *J. Neurosci.* 14:5160–5169.

Isom, L.I., K.S. De Jongh, D.E. Patton, B.F.X. Reber, J. Offord, H. Charbonneau, K. Walsh, A.L. Goldin, and W.A. Catterall. 1992. Primary structure and functional expression of the β1 subunit of the rat brain sodium channel. *Science (Wash. DC).* 256:839–842.

Isom, L.L., K.S. De Jongh, and W.A. Catterall. 1994. Auxiliary subunits of voltage-gated ion channels. *Neuron.* 12:1183–1193.

Jackson, F.R., S.D. Wilson, and L.M. Hall. 1986. The *tip-E* mutation of Drosophila decreases saxitoxin binding and interacts with other mutations affecting nerve membrane excitability. *J. Neurogen.* 3:1–17.

Kirsch, G.E., A. Skattebol, L.D. Possani, and A.M. Brown. 1989. Modification of Na channel gating by an α scorpion toxin from *Tityus serrulatus*. *J. Gen. Physiol.* 93:67–83.

Knaus, H.-G., K. Folander, M. Garcia-Calvo, M.L. Garcia, G.J. Kaczorowski, M. Smith, and R. Swanson. 1994. Primary sequence and immunological characterization of β-subunit of high conductance Ca^{2+}-activated K^+ channel from smooth muscle. *J. Biol. Chem.* 269:17274–17278.

Knipple, D.C., K.E. Doyle, P.A. Marsella-Herrick, and D.M. Soderlund. 1994. Tight genetic linkage between the *kdr* insecticide resistance trait and a voltage-sensitive sodium channel gene in the house fly. *Proc. Natl. Acad. Sci. USA.* 91:2483–2487.

Kontis, K.J., and A.L. Goldin. 1993. Site-directed mutagenesis of the putative pore region of the rat IIA sodium channel. *Mol. Pharmacol.* 43:635–644.

Krafte, D.S., A.L. Goldin, V.J. Auld, R.J. Dunn, N. Davidson, and H.A. Lester. 1990. Inactivation of cloned sodium channels expressed in Xenopus oocytes. *J. Gen. Physiol.* 96:689–706.

Krafte, D.S., and W.A. Volberg. 1992. Properties of endogenous voltage-dependent sodium currents in Xenopus laevis oocytes. *J. Neurosci. Methods* 43:189–193.

Laemmli, U.K. 1970. Cleavage of structural proteins during assembly of the head of bacteriophage T4. *Nature (Lond.).* 227:680–685.

Liu, D.T., G.R. Tibbs, and S.A. Siegelbaum. 1996. Subunit stoichiometry of cyclic nucleotide-gated channels and effects of subunit order on channel function. *Neuron.* 16:983–990.

Loughney, K., R. Kreber, and B. Ganetzky. 1989. Molecular analysis of the *para* locus, a sodium channel gene in Drosophila. *Cell.* 58: 1143–1154.

Makita, N., P.B. Bennett, and A.L. George. 1994. Voltage-gated Na^+ channel β_1 subunit messenger RNA expressed in adult human skeletal muscle, heart and brain is encoded by a single gene. *J. Biol. Chem.* 269:7571–7578.

McManus, O.B., L.M. Helms, L. Pallanck, B. Ganetzky, R. Swanson,

and R.J. Leonard. 1995. Functional role of the beta subunit of high conductance calcium-activated potassium channels. *Neuron.* 14:645–650.

Miyazaki, M., K. Ohyama, D.Y. Dunlap, and F. Matsumura. 1996. Cloning and sequencing of the *para*-type sodium channel gene from susceptible and *kdr*-resistant German cockroaches (*Blattella germanica*) and house fly (*Musca domestica*). *Mol. Gen. Genet.* 252: 61–68.

Moorman, J.R., G.E. Kirsch, A.M. Vandongen, R.H. Joho, and A.M. Brown. 1990. Fast and slow gating of sodium channels encoded by a single mRNA. *Neuron.* 4:243–252.

Narahashi, T. 1992. Nerve membrane Na^+ channels as targets of insecticides. *Trends Pharmacol. Sci.* 13:236–241.

Narahashi, T. 1996. Neuronal ion channels as the target sites of insecticides. *Pharmacol. Toxicol.* 78:1–14.

Norton, R.S. 1991. Structure and structure-function relationships of sea anemone proteins that interact with the sodium channel. *Toxicon.* 29:1051–1084.

O'Dowd, D.K. 1995. Voltage-gated currents and firing properties of embryonic Drosophila neurons grown in a chemically defined medium. *J. Neurobiol.* 27:113–126.

O'Dowd, D.K., and R.W. Aldrich. 1988. Voltage-clamp analysis of sodium channels in wild-type and mutant Drosophila neurons. *J. Neurosci.* 8:3633–3643.

O'Dowd, D.K., J.R. Gee, and M.A. Smith. 1995. Sodium channel density correlates with expression of specific alternatively spliced sodium channel mRNAs in single neurons. *J. Neurosci.* 15:4005–4012.

Pallanck, L., and B. Ganetzky. 1994. Cloning and characterization of human and mouse homologs of the Drosophila calcium-activated potassium channel gene, *slowpoke. Hum. Mol. Genet.* 3:1239–1243.

Patton, D.E., L.L. Isom, W.A. Catterall, and A.L. Goldin. 1994. The adult rat brain β_1 subunit modifies activation and inactivation gating of multiple sodium channel α subunits. *J. Biol. Chem.* 269: 17649–17655.

Pauron, D., J. Barhanin, and M. Lazdunski. 1985. The voltage-dependent Na^+ channel of insect nervous system identified by receptor sites for tetrodotoxin, and scorpion and sea anemone toxins. *Biochem. Biophys. Res. Commun.* 131:1226–1233.

Qu, Y., L.L. Isom, R.E. Westenbroek, J.C. Rogers, T.N. Tanada, K.A. McCormick, T. Scheuer, and W.A. Catterall. 1995. Modulation of cardiac Na^+ channel expression in Xenopus oocytes by β1 subunits. *J. Biol. Chem.* 270:25696–25701.

Ramaswami, M., and M. Tanouye. 1989. Two sodium channel genes in Drosophila: implications for channel diversity. *Proc. Natl. Acad. Sci. USA.* 86:2079–2082.

Rettig, J., S.H. Heinemann, F. Wunder, C. Lorra, D.N. Parcej, J.O. Dolly, and O. Pongs. 1994. Inactivation properties of voltage-gated K^+ channels altered by presence of beta subunit. *Nature (Lond.).* 369:289–294.

Ritchie, J.M., and R.B. Rogart. 1977. The binding of saxitoxin and tetrodotoxin to excitable tissue. *Rev. Physiol. Biochem. Pharmacol.* 79:1–51.

Rogers, J.C., Y. Qu, T.N. Tanada, T. Scheuer, and W.A. Catterall. 1996. Molecular determinants of high affinity binding of α-scorpion toxin and sea anemone toxin in the S3-S4 extracellular loop in domain IV of the Na^+ channel α subunit. *J. Biol. Chem.* 271: 15950–15962.

Saito, M., and C.-F. Wu. 1993. Ionic channels in cultured Drosophila neurons. Birkhauser Verlag, Basel, Switzerland.

Sambrook, J., E.F. Fritsch, and T. Maniatis. 1989. Molecular Cloning: A Laboratory Manual. Cold Spring Harbor Laboratory Press, Cold Spring Harbor, New York.

Song, J.-H., and T. Narahashi. 1996. Modulation of sodium channels of rat cerebellar Purkinje neurons by the pyrethroid tetramethrin. *J. Pharmacol. Exp. Ther.* 277:445–453.

Taglialatela, M., L. Toro, and E. Stefani. 1992. Novel voltage clamp to record small, fast currents from ion channels expressed in Xenopus oocytes. *Biophys. J.* 61:78–82.

Tatebayashi, H., and T. Narahashi. 1994. Differential mechanism of action of the pyrethroid tetramethrin on tetrodotoxin-sensitive and tetrodotoxin-resistant sodium channels. *J. Pharmacol. Exp. Ther.* 270:595–603.

Taylor, M.F.J., D.G. Heckel, T.M. Brown, M.E. Kreitman, and B. Black. 1993. Linkage of pyrethroid insecticide resistance to a sodium channel locus in the tobacco budworm. *Insect Biochem. Mol. Biol.* 23:763–775.

Terlau, H., S.H. Heinemann, W. Stuhmer, W. Pusch, F. Conti, K. Imoto, and S. Numa. 1991. Mapping the site of block by tetrodotoxin and saxitoxin of sodium channel II. *FEBS Lett.* 293:93–96.

Thackeray, J.R., and B. Ganetzky. 1994. Developmentally regulated alternative splicing generates a complex array of Drosophila para sodium channel isoforms. *J. Neurosci.* 14:2569–2578.

Vijverberg, H.P.M., and J. van den Bercken. 1990. Neurotoxicological effects and the mode of action of pyrethroid insecticides. *Crit. Rev. Toxicol.* 21:105–126.

Vijverberg, H.P.M., J.M. van der Zalm, R.G.D.M. van Kleef, and J. van den Bercken. 1983. Temperature- and structure-dependent interaction of pyrethroids with the sodium channels in frog node of Ranvier. *Biochim. Biophys. Acta.* 728:73–82.

West, J.W., D.E. Patton, T. Scheuer, Y. Wang, A.L. Goldin, and W.A. Catterall. 1992. A cluster of hydrophobic amino acid residues required for fast Na^+-channel inactivation. *Proc. Natl. Acad. Sci. USA.* 89:10910–10914.

Williamson, M.S., I. Denholm, C.A. Bell, and A.L. Devonshire. 1993. Knockdown resistance (*kdr*) to DDT and pyrethroid insecticides maps to a sodium channel gene locus in the housefly (*Musca domestica*). *Mol. Gen. Genet.* 240:17–22.

Zhou, J., J.F. Potts, J.S. Trimmer, W.S. Agnew, and F.J. Sigworth. 1991. Multiple gating modes and the effect of modulating factors on the μI sodium channel. *Neuron.* 7:775–785.

Zong, X.-G., M. Dugas, and P. Honerjager. 1992. Relation between veratridine reaction dynamics and macroscopic Na current in single cardiac cells. *J. Gen. Physiol.* 99:683–697.